Desalination and Water Treatment
www.deswater.com
doi: 10.5004/dwt.2022.29105

279 (2022) 173–177
December

Effect of Reynolds number on turbulence characteristics of turbulent Ostwald–de Waele fluids

Mohamed Abdi[a,*], Meryem Ould-Rouiss[b], Lalia Abir Bouhenni[c], Nour Elhouda Beladjine[c], Belhouari Abdelkarim Bekhtaoui[c]

[a]*Laboratoire de génie électrique et des plasmas (LGEP), University of Tiaret, Algeria, email: abdi.mohamed1@live.fr (M. Abdi)*
[b]*Laboratoire de Modélisation et Simulation Multi Echelle, MSME, Université Gustave Eiffel, UMR 8208 CNRS, 5 bd Descartes, 77454 Marne-la-Vallée, Paris, France*
[c]*Department of Mechanical Engineering, University Ibn Khaldoun, Tiaret 14000, Algeria*

Received 19 April 2022; Accepted 25 September 2022

ABSTRACT

The current work aimed to understand how the Reynolds number affected the characteristics of turbulent power-law fluids. A fully developed large-eddy simulation of turbulent pseudoplastic and dilatant fluids over a straight pipe was performed numerically at three Reynolds numbers (4,000; 8,000 and 12,000) and flow behaviour indexes of (0.75, 1 and 1.4). The key findings indicated that when the Reynolds number rose, the creation of axial fluctuations close to the wall area was amplified significantly. This led to a notably improved kinetic energy of turbulent fluctuations across the radial direction. The mechanism of the velocity variations from the near-wall area towards the core region was enhanced with rising Reynolds numbers. This trend was more evident as the flow behaviour index dropped.

Keywords: Large-eddy simulation; Shear-thinning; Shear-thickening; Turbulence

1. Introduction

Non-Newtonian flow plays a significant role in the mechanical and engineering sectors, particularly in processing food, pharmaceuticals, polymers, cement, petroleum, and other materials. In the last several decades, research on the power-law fluids in pipe designs has generated a significant quantity of literature, most of which has focused on the turbulent flow of non-Newtonian fluids [1–12]. For the first time, Dodge and Metzner [3], in their article, reported a theoretical analysis turbulent flow of non-Newtonian fluids through smooth pipes. With four concentrations of a polymer shear-thinning solution (sodium carboxymethyl cellulose) and water, Pinho and Whitelaw [5] assessed the mean axial velocity and the three normal stresses in fully developed pipe flow across a range of Reynolds numbers from 240 to 111,000. Direct numerical simulation (DNS) was carried out by Gavrilov and Rudyak [10,11] at two generalised Reynolds values, 10,000 and 20,000, across power-law index ranges of 0.4 to 1. Recently, Singh et al. [12] used (DNS) at a friction Reynolds number Re_τ = 323 to examine the impact of the flow index parameter of power-law fluids in turbulent pipe flow.

In a more recent study, Abdi et al. [13] used large-eddy simulation (LES) and an extended Smagorinsky model to perform fully developed turbulent forced convection of thermally independent pseudoplastic fluid via an axially heated rotating conduit. With a rotational speed ranging from 0 to 3,

* Corresponding author.

Presented at the First International Congress of Energy and Industrial Process Engineering (ICEIPE'22) 23–25 May 2022, Algiers, Algeria

the simulation is working fluid Reynolds and Prandtl values were set to 4,000 and 1, respectively. The temperature along the pipe wall radius is shown to fall as the rotation rate rises pipe wall rotates dramatically. This is due to a centrifugal force that substantially causes the mean axial velocity profile to rise when the apparent fluid viscosity in the pipe core region lowers.

In the current study, with a typical dynamic model and the LES technique, a numerical analysis of the fully developed turbulent flow of power-law fluids through a pipe was carried out for three simulations of Reynolds values (Re_s = 4,000; 8,000 and 12,000). The flow behaviour indices used in this research primarily examined pseudoplastic and dilatant fluids were 0.75 (shear-thinning), 1, and 1.4, respectively (shear-thickening). The investigation aimed to demonstrate how the Reynolds number affected the turbulence characteristics through analysis and discussion of the key turbulence statistics related to these problems.

2. Governing equations and numerical procedure

2.1. Governing equations

The present study was devoted to a fully developed turbulent flow of pseudoplastic (n = 0.75), dilatant (n = 1.4) and Newtonian (n = 1) fluids through an axially stationary pipe with a computational domain of 20R (Fig. 1) by employing LES with a standard dynamic model. Three simulation Reynolds numbers (Re_s) were considered (4,000; 8,000 and 12,000), which were based on the centerline axial velocity of the analytical fully developed laminar profile (U_{CL}), which were defined respectively as $Re_s = \rho U_{CL}^{2-n} R^n / K$ and $U_{CL} = (3n + 1)U_b/(n + 1)$. The filtered equations can be expressed as follows:

$$\frac{\partial \overline{u}_i}{\partial x_i} = 0 \tag{1}$$

$$\frac{\partial \overline{u}_j}{\partial t} + \frac{\partial \overline{u}_i \overline{u}_j}{\partial x_i} = -\frac{d\overline{P}}{\partial x_j}\frac{1}{\mathrm{Re}_S}\frac{\partial}{\partial x_i}\left[\overline{\dot{\gamma}^{n-1}}\left(\frac{\partial \overline{u}_j}{\partial x_i} + \frac{\partial \overline{u}_i}{\partial x_j}\right)\right] + \frac{\partial \overline{\tau}_{ij}}{\partial x_i} \tag{2}$$

The constitutive equation for the power-law model is given by:

$$\tau = K\dot{\gamma}^n \tag{3}$$

The variables K and n are the fluid consistency index and the flow behaviour index, respectively. The shear-thinning behaviour occurs for n < 1, shear-thickening for n > 1, and n = 1 the fluid shows Newtonian behaviour.

2.2. Numerical procedure

The present investigation was performed with a grid resolution of 65^3 grid points in axial, radial and circumferential directions. The governing equations were discretised on a staggered mesh in cylindrical coordinates with a computational length in the axial direction 20R. The numerical integration was performed using a finite difference scheme, second-order accurate in space and time. The time advancement employed a fractional-step method. A third-order Runge–Kutta explicit scheme and a Crank–Nicolson implicit scheme were utilised to evaluate convective and diffusive terms. The above mathematical model was implemented in a finite difference laboratory code. In the non-Newtonian Smagorinsky model, the subgrid stress tensor $\overline{\tau}$ is linked to the strain rate tensor by $\overline{\tau}_{ij} = -2\nu_t \overline{S}_{ij}$. The turbulent viscosity is computed by $\nu_t = C_s f_s \left(f_n \Delta\right)^2 \overline{S}_{ij}$, where D is the computational filter, C_s the model constant, f_s the van driest wall damping function, and f_n is the correction function for the change in viscosity.

3. Results and discussion

The aim was to discern or distinguish the Reynolds number influence on the power-law fluids turbulence characteristics in turbulent pipe flow. The study was focused on the pseudoplastic (shear-thinning n = 0.75), dilatant (shear-thickening n = 1.4) and Newtonian (n = 1) fluids at low (Re_s = 4,000), moderate (Re_s = 8,000) and high (Re_s = 12,000) simulation Reynolds numbers. To ascertain the accuracy and reliability of the results, the turbulence intensities of the axial, radial and tangential velocity fluctuations of a Newtonian fluid compared reasonably with that of Redjem-Saad et al. [14] at the Reynolds number of 5,500. It was apparent that no significant difference was observed between the root mean square (RMS) profiles of the axial component, where the turbulence intensities of the axial velocity collapsed with that of Redjem-Saad et al. [14] along the radial coordinate. The turbulence intensities of the radial and tangential velocity fluctuations were slightly overestimated compared to those of Redjem-Saad et al. [14]. The small discrepancy may have been due to the difference in the Reynolds number value and the numerical solution procedure.

3.1. Turbulence intensities of velocity fluctuations

The RMS distributions of the axial, radial and tangential velocity fluctuations along the pipe radius vs. the distance from the wall in wall units Y^+ scaled by the friction velocity are presented respectively in Figs. 2 and 5. As appears in Fig. 2, the turbulence intensities of the axial velocity fluctuations were almost identical over the near-wall region (Y^+ < 3) for all studied cases, which was due to the absence

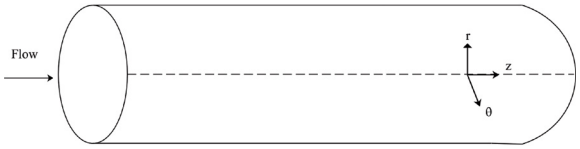

Fig. 1. Computational domain.

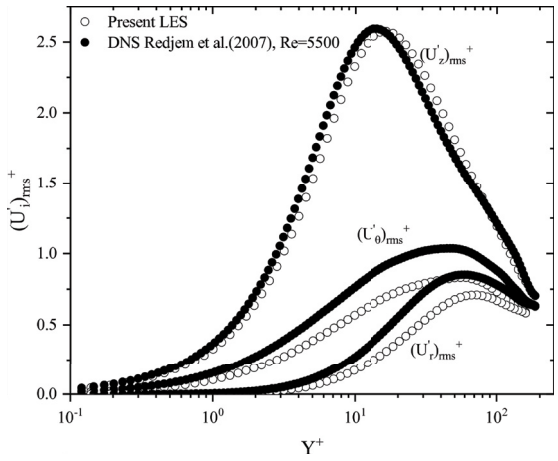

Fig. 2. Validation of the results.

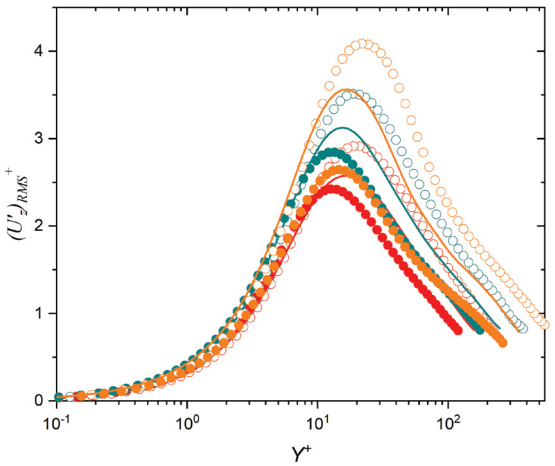

Fig. 3. RMS of axial component vs. Y^+. Open symbols: n = 0.75; solid line: n = 1; closed symbols: n = 1.4; Red: Re_s = 4,000; Blue: Re_s = 8,000; Orange: Re_s = 12,000.

of turbulent shear stress where the molecular shear stress force was dominant in this flow region. Beyond approximately (Y^+ = 5), the profiles increased and deviated from each other gradually the further away from the wall with the wall distance Y^+. The axial turbulence intensities began to enhance significantly beyond (Y^+ = 5), which indicated that the axial velocity fluctuations were generated in the near-wall region. There was a clear trend of increasing axial turbulence intensities along the radial direction out of the viscous sublayer ($0 \le Y^+ \le 5$). This meant the axial fluctuations propagated from the wall towards the remaining flow regions. Beyond approximately (Y^+ = 20), the axial turbulence intensities began to drop progressively towards the core region. These profiles fell to lower values in the core region for all cases. In other words, the axial velocity fluctuations gradually vanished with the logarithmic region wall distance ($30 \le Y^+ \le 200$).

It can be seen from Fig. 2 that the axial turbulence intensities profiles of the Reynolds number of 12,000 were considerably larger than those of 8,000 and 4,000 along the radial direction for all flow behaviour indices, especially at the peak value location. The increased Reynolds number also led to shifting the peak location from the wall towards the core region. It can be said that the increased Reynolds number resulted in a pronounced enhancement in the generation of axial fluctuations near the wall region, which also led to ameliorating the transport of these fluctuations from the viscous sublayer towards the core region along the radial direction. It was worth noting that this trend was more pronounced as the flow behaviour index (n) decreased. On the other hand, the RMS profiles of the shear-thinning fluids lay above those of the shear-thickening and Newtonian fluids along the pipe radius. This meant that the decreased flow behaviour index (n) led to improving the generation and the propagation of the axial fluctuations along the radial direction, as pointed out by Gavrilov and Rudyak [10], where this trend was more pronounced as the Reynolds number increased.

As appears in Fig. 3, the turbulence intensities of the radial velocity fluctuations were nearly linear and equal to zero value along the near-wall region ($Y^+ < 3$) for all cases. It can be said that the RMS of the radial component was nearly independent of the Reynolds number and the flow behaviour index in this region. At a large wall distance, the effects of the Reynolds number and flow behaviour index became more significant with the wall distance. The radial turbulence intensities began to increase gradually far away from the wall with wall distance Y^+. Moreover, these profiles began also to deviate from each other out of the viscous sublayer ($0 \le Y^+ \le 5$), where this deviation became more distinct with increasing Reynolds number. Out of the buffer region ($5 \le Y^+ \le 30$), the radial turbulence intensities profiles began to decrease noticeably after reaching their peak values in the logarithmic region ($30 \le Y^+ \le 200$) for the three Reynolds numbers.

As shown in Fig. 3, the profiles of the 12,000 lay slightly below those of the 8,000 and 4,000 along the pipe radius. These profiles of 12,000 appeared to shift away from the wall towards the core region as compared with those of 8,000 and 4,000 for all flow behaviour indices. It was evident that the increased Reynolds number led to attenuating or lessening the radial turbulence intensities slightly and also led to improving the propagation of these fluctuations from the wall to the core region. This trend was more pronounced as the flow behaviour index decreased. On the other hand, the pseudoplastic (n = 0.75) profiles lie down those of the dilatant (n = 1.4) and Newtonian fluid for all Reynolds numbers along the radial coordinate, where the decreased flow behaviour index results in a marked attenuation in the radial turbulence intensities over the pipe radius, as pointed out by Gavrilov and Rudyak [10].

Fig. 4 shows the distribution of turbulence intensities of the tangential velocity fluctuations. These profiles had the same trend over the pipe radius, where there was a clear trend of oscillations in this profile along the radial direction for Reynolds numbers of 4,000; 8,000 and 12,000 for the three flow behaviour indices. It can be said that the tangential turbulence intensities were less affected by the Reynolds number, where it was apparent that no significant noteworthy differences were found between the profiles of 1,200; 8,000 and 4,000 along the radial direction for the three flow behaviour indices.

3.2. Turbulent kinetic energy

The kinetic energy of turbulent fluctuations of the pseudoplastic (n = 0.75), dilatant (n = 1.4) and Newtonian (n = 1) fluids along the pipe radius (R) are illustrated in Fig. 5. The turbulent kinetic energy profile was linear and remained constant in the near-wall region ($Y^+ < 1$) for all Reynolds numbers because of the absence of velocity fluctuations in the near-wall region. Far away from the wall, the turbulent kinetic energy began to enhance gradually with the wall distance Y^+. This enhancement or improvement was related to augmentation in the turbulence intensities of the axial, radial and tangential velocity fluctuations in this flow region. The turbulent kinetic energy profiles reached their peak values. Beyond approximately (Y^+ = 20), these profiles dropped rapidly to zero in the core region for all cases. This reduction occurred because of the vanishing of the axial, radial and tangential turbulence intensities in this flow region.

Interestingly, the axial velocity fluctuations were generated in the near-wall region (Fig. 2) and transferred to the radial and tangential components. These fluctuations vanished in the core region (Figs. 3 and 4), as pointed out by Gavrilov and Rudyak [10]. As shown in Fig. 5 the turbulent kinetic energy profile of the Reynolds number of 12,000 lies above those of 8,000 and 4,000 along the pipe radius, especially in the buffer region. The increased Reynolds number resulted in an enhancement in the generation of the axial fluctuations. The transfer mechanism of these fluctuations to the radial and tangential components consequently ameliorated the kinetic energy of turbulent fluctuations over the radial direction. It should be noted that this trend was more pronounced as the flow behaviour index increased.

3.3. Turbulent Reynolds shear stress

The predicted profiles of Reynolds shear stress were equal to zero along the viscous sublayer ($0 \le Y^+ \le 5$). These profiles deviated significantly from each other and exhibited a gradual enhancement with wall distance. Beyond the logarithmic region ($30 \le Y^+ \le 200$), these profiles dropped to zero in the core region. It was evident that the increased Reynolds number resulted in a marked enhancement in the

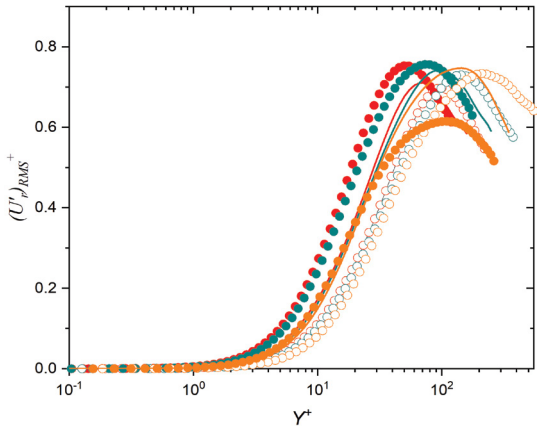

Fig. 4. RMS of the radial component against Y^+. Open symbols: n = 0.75; solid line: n = 1; closed symbols: n = 1.4; Red: Re_s = 4,000; Blue: Re_s = 8,000; Orange: Re_s = 12,000.

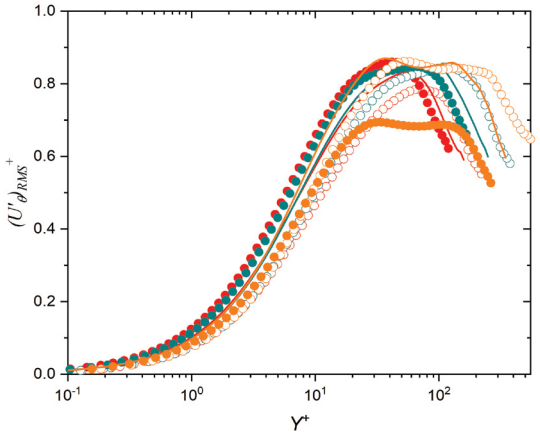

Fig. 5. RMS of the tangential component vs. Y^+. Open symbols: n = 0.75; solid line: n = 1; closed symbols: n = 1.4; Red: Re_s = 4,000; Blue: Re_s = 8,000; Orange: Re_s = 12,000.

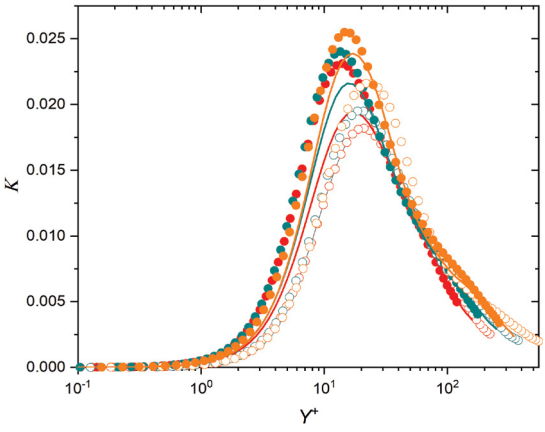

Fig. 6. Turbulent kinetic energy against Y^+. Open symbols: n = 0.75; solid line: n = 1; closed symbols: n = 1.4; Red: Re_s = 4,000; Blue: Re_s = 8,000; Orange: Re_s = 12,000.

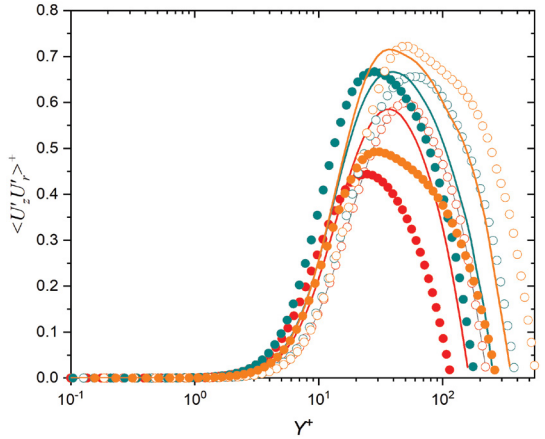

Fig. 7. Turbulent Reynolds stress vs. Y^+. Open symbols: n = 0.75; solid line: n = 1; closed symbols: n = 1.4; Red: Re_s = 4,000; Blue: Re_s = 8,000; Orange: Re_s = 12,000.

Reynolds stress, especially in the logarithmic region, for the three flow behaviour indices.

4. Conclusions

The current study focused on the numerical analysis of a fully developed turbulent flow of power-law fluids in a conduit using the LES technique and a conventional dynamic model at three Reynolds number simulations (4,000; 8,000 and 12,000). With flow behaviour indices of 0.75 and 1.4, respectively, this research sought to determine the effect of the Reynolds number on the mean turbulence characteristics of turbulent pseudoplastic and dilatant fluids. The results indicated that radial turbulence intensities were attenuated, and the higher Reynolds number significantly enhanced the axial fluctuations near the wall area. Additionally, the higher Reynolds number facilitated the radial transmission of these variations from the viscous sublayer to the core area. These trends became more evident as the flow behaviour index dropped. An increase in Reynolds number enhanced the kinetic energy of turbulent variations in the radial direction. This tendency became more evident as the flow behaviour index rose.

Symbols

U_b	—	Average velocity, m·s^{-1}
U_τ	—	Friction velocity $U_\tau = (\tau_w/\rho)^{1/2}$, m·s^{-1}
U_{CL}	—	Centreline axial velocity for analytical fully developed laminar profile $U_{CL} = (3n + 1)U_b/(n + 1)$, m·s^{-1}
R	—	Pipe radius, m
n	—	Flow index
K	—	Consistency index, Pa·s^n
Y^+	—	Wall distance $Y^+ = \rho U_\tau Y/\eta_w$
f	—	Friction factor $f = 2\tau_w/(\rho U_b^2)$
Re_s	—	Reynolds number of the simulations $\mathrm{Re}_s = \rho U_{CL}^{2-n} R^n/K$

Greek symbols

$\nu_t = C_s f_s \left(f_n \Delta\right)^2 \overline{S}_{ij}$	—	Shear rate $\dot{\gamma} = \sqrt{S_{ij} S_{ij}}$
η	—	Apparent viscosity $\eta = K\dot{\gamma}^{n-1}$
ρ	—	Density
$\overline{\tau}_{ij}$	—	Subgrid stress tensor $\overline{\tau}_{ij} = -2\nu_t \overline{S}_{ij}$

Subscripts

z, r, θ	—	Axial, radial, tangential velocity
C	—	Centreline
L	—	Laminar
s	—	Simulation
w	—	Wall

Superscripts

$\langle\ \rangle$	—	Statistically averaged
$(\ )^+$	—	Normalised by U_τ

References

[1] A.B. Metzner, J.C. Reed, Flow of non-Newtonian fluids—correlation of the laminar, transition, and turbulent-flow regions, AlChE J., 1 (1955) 434–440.

[2] A.B. Metzner, Non-Newtonian fluid flow. Relationships between recent pressure-drop correlations, Ind. Eng. Chem., 49 (1957) 1429–1432.

[3] D.W. Dodge, A.B. Metzner, Turbulent flow of non-Newtonian systems, AIChE J., 5 (1959) 189–204.

[4] V. Vidyanidhi, A. Sithapathi, Non-Newtonian flow in a rotating straight pipe, J. Phys. Soc. Jpn., 29 (1970) 215–219.

[5] F.T. Pinho, J.H. Whitelaw, Flow of non-Newtonian fluids in a pipe, J. Non-Newtonian Fluid Mech., 34 (1990) 129–144.

[6] M.R. Malin, Turbulent pipe flow of power-law fluids, Int. Commun. Heat Mass Transfer, 24 (1997) 977–988.

[7] M.R. Malin, The turbulent flow of Bingham plastic fluids in smooth circular tubes, Int. Commun. Heat Mass Transfer, 24 (1997) 793–804.

[8] T. Ohta, M. Miyashita, DNS and LES with an extended Smagorinsky model for wall turbulence in non-Newtonian viscous fluids, J. Non-Newtonian Fluid Mech., 206 (2014) 29–39.

[9] P.S. Gnambode, P. Orlandi, M. Ould-Rouiss, X. Nicolas, Large-Eddy simulation of turbulent pipe flow of power-law fluids, Int. J. Heat Fluid Flow, 54 (2015) 196–210.

[10] A.A. Gavrilov, V.Y. Rudyak, Direct numerical simulation of the turbulent flows of power-law fluids in a circular pipe, Thermophys. Aeromech., 23 (2016) 473–486.

[11] A.A. Gavrilov, V.Ya. Rudyak, Direct numerical simulation of the turbulent energy balance and the shear stresses in power-law fluid flows in pipes, Fluid Dyn., 52 (2017) 363–374.

[12] J. Singh, M. Rudman, H.M. Blackburn, The effect of yield stress on pipe flow turbulence for generalised Newtonian fluids, J. Non-Newtonian Fluid Mech., 249 (2017) 53–62.

[13] M. Abdi, A. Noureddine, M. Ould-Rouiss, Numerical simulation of turbulent forced convection of a power law fluid flow in an axially rotating pipe, J. Braz. Soc. Mech. Sci., Eng., 42 (2020) 17, doi: 10.1007/s40430-019-2099-7.

[14] L. Redjem-Saad, M. Ould-Rouiss, G. Lauriat, Direct numerical simulation of turbulent heat transfer in pipe flows: effect of Prandtl number, Int. J. Heat Fluid Flow, 28 (2007) 847–861.